ACS OMEGA

http://pubs.acs.org/journal/acsodf

Article

Nanopath-Beacons for Directed Silver Dendrites' Migration across Graphene Oxide Terrain

Lu Gan, Sharon Xiaodai Lim,* and Chorng-Haur Sow*

Cite This: *ACS Omega* 2022, 7, 10330−10339

Read Online

ACCESS | Metrics & More | Article Recommendations

ABSTRACT: With their special hierarchical fractal and highly symmetric formation, silver dendrites have a large surface area and plentiful active sites at edges, which have allowed them to exhibit unique properties ranging from superhydrophobic surfaces to biosensors. Yet, many suggested synthesis processes either require a long reaction time or risk contamination from sacrificial elements. Limited research in directing while enhancing the growth of these silver dendrites also hinders the application of these unique microstructures as site-selective hydrophobicity of surfaces and location-dependent SERS (surface-enhanced Raman spectroscopy). A possible solution to this is to utilize WO_3 nanocubes as beacons to accelerate and conduct the growth of these silver dendrites through the electrochemical migration process. These nanocubes effortlessly altered the applied electric field distributed between the electrodes, depending on their orientations and positions. As the silver dendrites branched from the nanocubes, the dendrites themselves further concentrated the electric field to encourage the growth of more loose fractal silver dendrites. The combinatory effect successfully directs the growth of silver dendrites along the concentrated electric field paths. Both changes to the electric field and directed growth of silver dendrites are underscored using Multiphysics COMSOL simulations and time-lapse microscopy. This work provided insight into the possibility of designing microstructures to direct and accelerate the growth of silver dendrites.

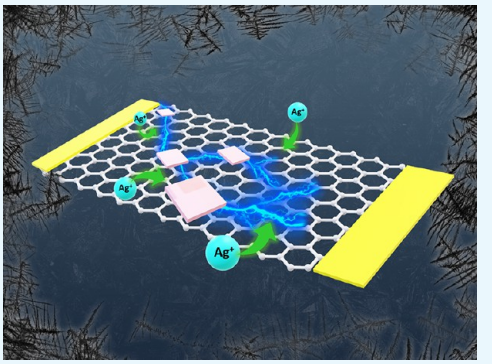

INTRODUCTION

For many decades, a wealth of nanostructures such as nanoparticles,[1] nanowire,[2] nanorods,[3] nanoflower,[4] and nanodendrites[5−7] have been fabricated from noble metals like copper,[8] gold,[9] palladium,[10] and silver.[6] By twitching with the sizes, crystallinities, shapes, and compositions, researchers have successfully coaxed unique properties out of these nanostructures. Of these nanostructures, nanodendrites with a special hierarchical fractal and highly symmetrical formation have rendered themselves distinctive. The large surface area and plentiful active sites at the edges of these nanodendrites allow them to form superhydrophobic[11] surfaces, produce surface-enhanced Raman scattering (SERS),[5,12] initiate catalytic processes,[9] and serve as biosensors.[13] Coincidentally, these nanodendrites displays far superior performance in SERS,[14] antibacterial ability,[15] and electrocatalysis[16] than their spherically shaped nanoparticles' counterparts.

Silver dendrites are highly sought after because of their excellent electrical and thermal conductivities among these noble metals. Furthermore, silver's electronic and optical properties are readily controlled by size and shape. So, to fabricate these silver dendrites, long-duration processes such as photoreduction in the presence of ultraviolet irradiation,[17] and the use of sacrificial metals such as copper and zinc in the galvanic replacement process,[5,18] has been well established. Although these processes can produce large amounts of silver dendrites, they cannot ascertain control over the direction of growth. Such control is critical to add more functionalities such as site-selective hydrophobicity of surfaces and location-dependent SERS to these amazing nanostructures.

Recently, some controls over these dendrites were reported with the implementation of templated-assisted growth during the galvanic replacement process.[19,20] Leow et al.[21] discovered that by running a focused laser beam along specific sites of the GO film, localized reduced GO (rGO) with higher conductivity can be created, which then encourages the electrochemical migration of silver dendrites along these paths. Regulated formation of Zn dendrites were also achieved by Sun et al. with the help of TiO_x/Zn/N-doped carbon inverse opal.[22]

With inheriting a large surface area to enhance the absorption of silver ions and concentrate aromatic molecules, a superior signal-to-noise ratio of silver dendrites coupled rGO in SERS application has also been reported.[23] GO is thus

Received: December 9, 2021
Accepted: February 28, 2022
Published: March 16, 2022

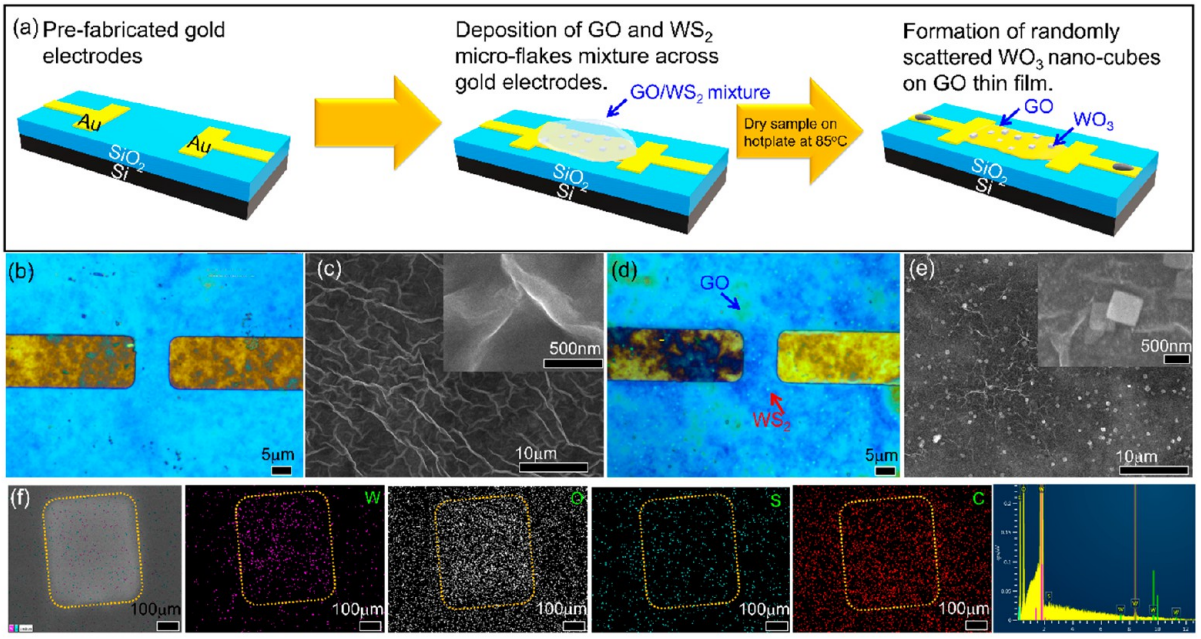

Figure 1. (a) Deposition of GO/WS_2 mixture across prefabricated gold electrodes. (b, d) Optical images of (b) Pristine GO film and (d) GO/WS_2 mixture being deposited across the gold electrodes. (c, e) SEM images of the (c) pristine GO film and (e) GO/WS_2 mixture. Insets of (c) and (e) show higher magnification of the GO film and nanocubes, respectively. (f) EDX elemental map of a single nanocube.

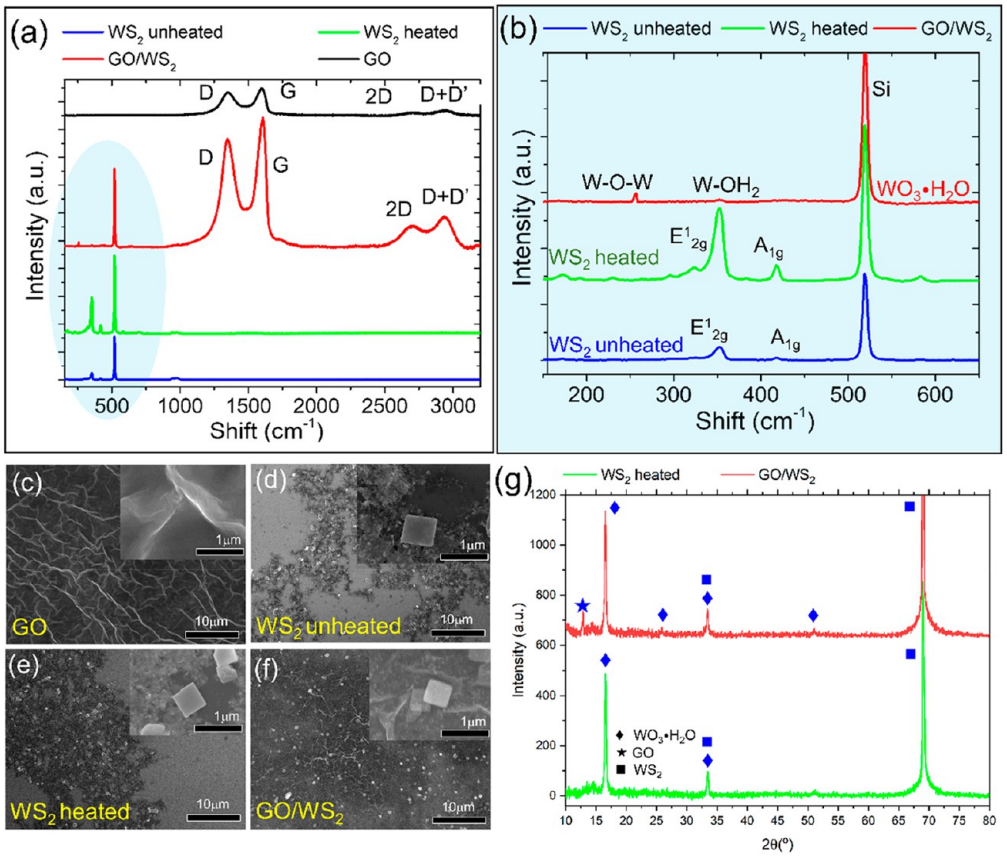

Figure 2. (a) Raman spectrum of pristine GO, pristine WS_2, heated WS_2, and GO/WS_2 mixture that has been heated to 85 °C. (b) An expanded view of the Raman measurement range between 150 cm^{-1} to 650 cm^{-1}. (c–f) SEM images of the samples used in the Raman measurement. Insets are images with higher magnifications of the respective samples. (g) XRD patterns of heated WS_2 and GO/WS_2 mixture.

selected as a potential candidate in our quest to develop a way to direct the growth of silver dendrites while enhancing their formations through electrochemical migration. This is an aim that has yet to be accomplished. The decision to investigate

https://doi.org/10.1021/acsomega.1c06963
ACS Omega 2022, 7, 10330−10339

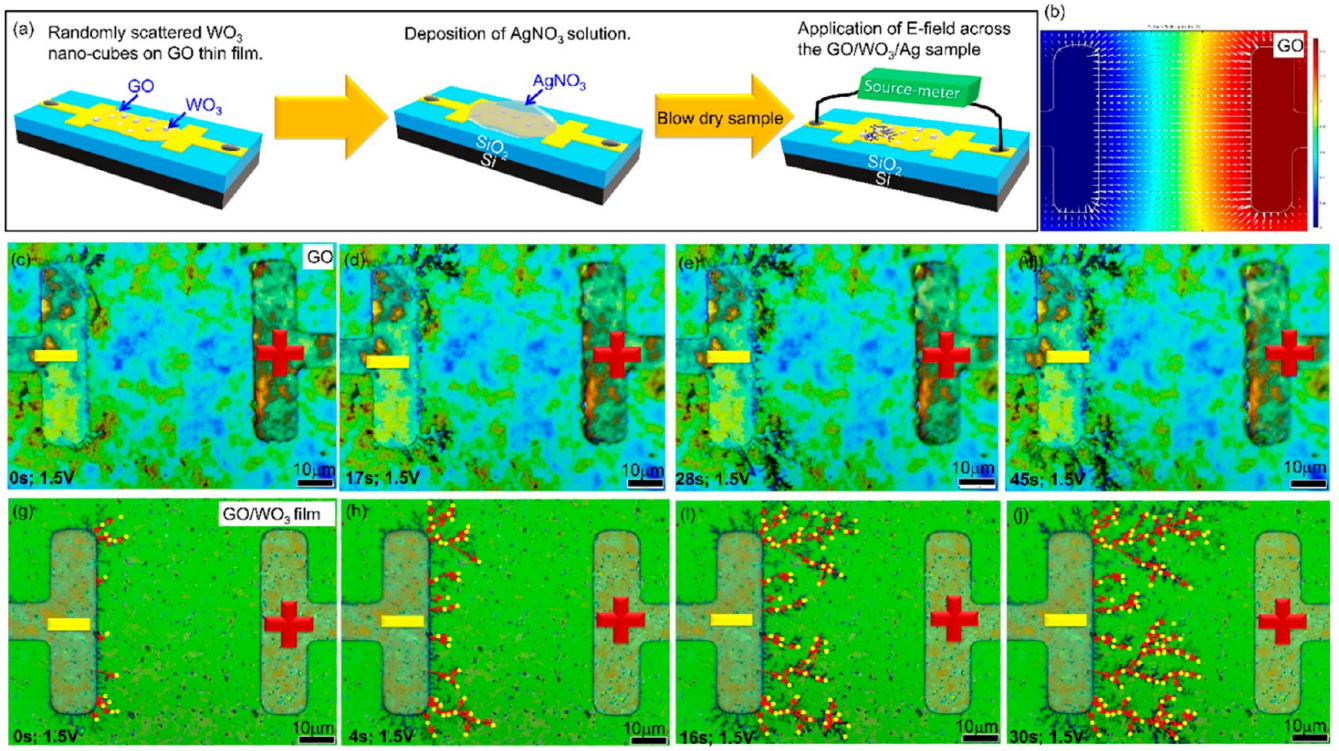

Figure 3. (a) Schematic of the fabrication process in which the $AgNO_3$ solution is deposited on GO/WO_3 film. (b) COMSOL simulation of electric field lines between two T-shaped electrodes. Optical time-lapsed images of Ag migration under a constant voltage 1.5 V across GO film in the (c–f) absence and (g–j) presence of WO_3 nanocubes.

with an electrochemical migration[24] process lies in the advantages that this procedure has in creating a large scale, one-step synthesis process with good morphological control of the silver dendrites via a simple process of varying concentration of silver ions, current density, and deposition time.

Coincidentally, monolayer or few-layer tungsten disulfide (WS_2) has been discovered to form stable composites with metal nanoparticles[25] while improving the composite's overall electrochemical properties. These two-dimensional lamellar transition metal dichalcogenide (TMD) microflakes have a similar microstructure as GO, which will likely allow them to form a good composite with the GO flakes. As a result, the composite can produce a hybrid thin film with unique electric field distribution along the large surface area. In the presence of silver ions and under an applied potential, redistribution of these electric fields will encourage the formation of silver dendrites through an enhanced electrochemical process and direct the growth of these silver dendrites along these electric field lines.

In this work, WS_2 microflakes are intentionally mixed with a GO microflakes' suspension and deposited on silicon dioxide wafers to form a thin composite film. The intended strategy is to use these WS_2 microflakes as nanopath-beacons to guide the migration of the silver dendrites across the GO terrain. The composite film is then subjected to an applied potential in the presence of silver ions that are likely trapped between the microflakes. Multiphysics COMSOL simulation is then used to form a deeper understanding of how the redistribution of the electric field across the composite film can affect the establishment of these silver dendrites.

RESULTS AND DISCUSSION

Formation of GO/WO_3 Nanocubes' Composite Film. First, 0.9 μL of a diluted GO and WS_2 microflakes' solution is deposited between the prefabricated gold electrodes. The substrate with the solution is heated at 85 °C on a hot plate in ambient conditions until dry (Figure 1a). The outcome of these processes results in randomly scattered nanocubes on the composite thin film.

Figure 1b,c shows optical and SEM images of the pristine GO film, with a distinct optical contrast compared to the GO/WS_2 composite film. While GO film appears to be smooth with some crease (inset of Figure 1c), small white specks are observed to be sparsely scattered across the GO/WS_2 composite film (Figure 1d,e). Detailed SEM analysis shows a distinct cubic structure (inset Figure 1e) observed from these sparks. EDX elemental map of one of these cubes suggests that they are likely to be tungsten oxide (WO_3) nanocubes.

With only GO and WS_2 as the precursors, it is important to determine the chemical nature of the nanocubes and how they are formed via the process illustrated in Figure 1a. A nondestructive optical analysis is first carried out on these nanocubes using Raman spectroscopy (Figure 2a). The analysis involved four different sample types of film. Namely, pristine GO nanoflakes, pristine WS_2, heated WS_2, and heated GO/WS_2 films. Survey scan from 100 to 3200 cm^{-1} shows the presence of defects (D), graphitic (G), 2D and D+D′ peaks, all contributed by the GO flakes.[26] At the same time, samples with WS_2 shows a few distinct peaks below 600 cm^{-1} (highlighted by the blue oval).

Figure 2b shows an expanded view of the region highlighted by the blue oval in Figure 2a. Raman peak located at 518 cm^{-1} is associated with the underlying Si wafer.[26] The outcome

https://doi.org/10.1021/acsomega.1c06963
ACS Omega 2022, 7, 10330−10339

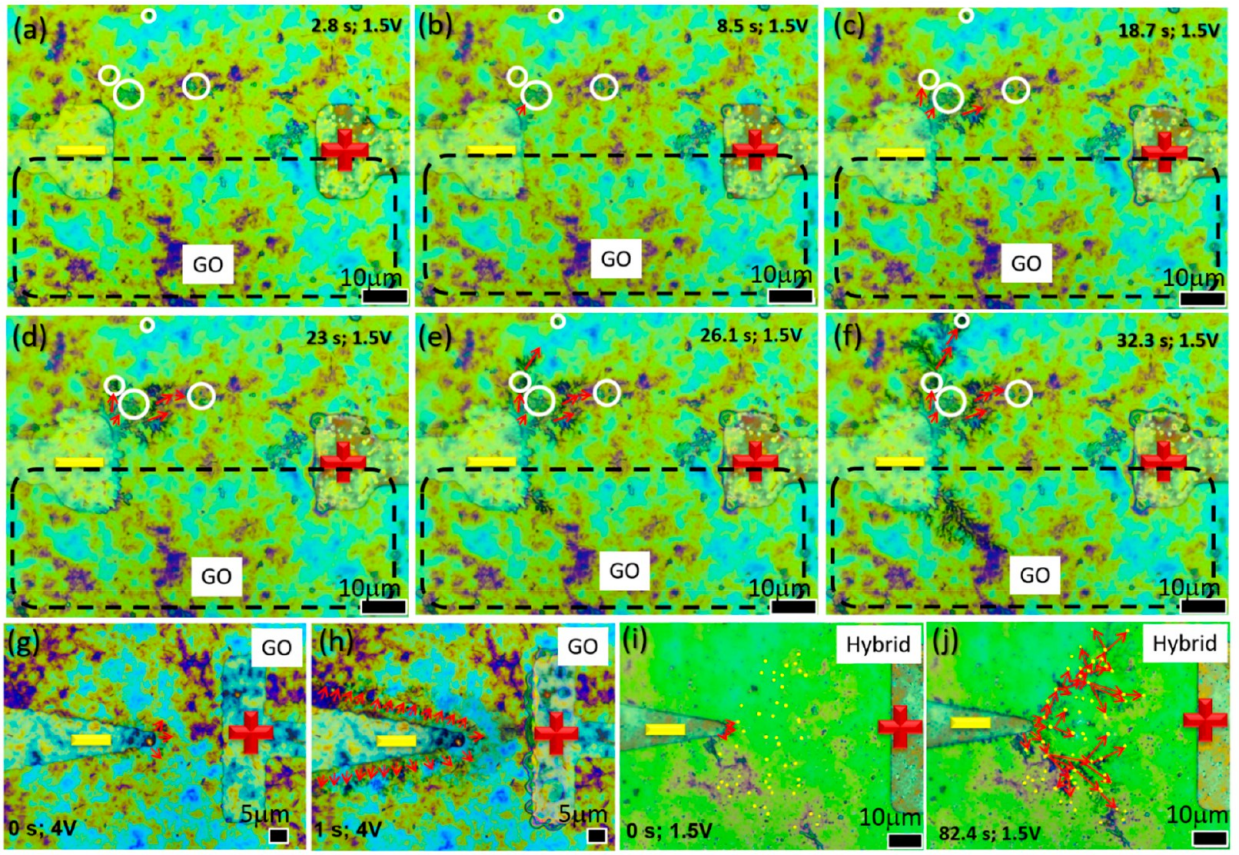

Figure 4. Time lapsed optical images of preferential growth of Ag dendrites in the presence of WO_3 nanocubes across (a–f) two T-shaped electrodes and (g–j) a combination of pointed and T-shaped electrodes. Red arrows and white circles in (a–f) demarked the Ag dendrites' growth and location of the WO_3 nanocubes, respectively. The black dotted line encloses a region with only pristine GO film in (a–f). (g–j) Time-lapsed optical images of Ag dendrites on (g,h) pristine GO film and (i,j) in the presence of WO_3 nanocubes. Yellow dots in (i) and (j) indicates the position of the WO_3 nanocubes.

suggests that strong Raman signals at ∼352 and ∼417 cm^{-1} represent the E^1_{2g} and A_{1g} modes in WS_2[27] unheated nanocubes in the absence of GO flakes. Evidently, after heating to 85 °C in ambient, more Raman peaks are detected. These peaks include those located at ∼295 and ∼323 cm^{-1}, which are associated with the $2E^2_{2g}$ and E^2_{2g} mode of WS_2.[27] presence of more peaks are attributed to heat-initiated dissociation of foreign molecules, which might have hindered the detection of pristine WS_2 Raman signals. As observed from the SEM images (Figure 2d,e), these occur without significant changes to the nanocubes' physical morphology. Figure 2c–f shows SEM images of pristine GO nanoflakes, pristine WS_2, heated WS_2, and heated GO/WS_2 films taken at similar magnifications. The insets of these show higher magnification SEM images of the respective samples.

Interestingly, with the addition of the GO flakes to the WS_2 nanocubes (Figure 2f), WS_2 Raman peaks are no longer detected. Instead, two distinct peaks located at ∼257 cm^{-1} (W–O–W bond) and ∼352 cm^{-1} (W–OH_2 bond), representative of $WO_3{\cdot}H_2O$ elements, are detected (Figure 2b).[28] The identified element, $WO_3{\cdot}H_2O$, also corresponded to the XRD pattern obtained from the GO/WS_2 mixture (Figure 2g), where the peak at 2θ = 12.8° corresponds to the (002) of GO sheets. The peaks at 2θ = 16.5°, 25.7°, 33.4°, and 51.2° are indexed to the diffraction pattern of orthorhombic $WO_3{\cdot}H_2O$ (JCPDS Card No. 43-0679). Because of incomplete conversion of WS_2 to $WO_3{\cdot}H_2O$, some XRD peaks associated with WS_2 are also identified at 2θ = 33.4°, 69.1° (JCPDS Card No. 35-06511). It is important to note that the XRD peak with a value of 2θ = 33.4 is being associated with both elements. Compared with heated WS_2 samples, XRD patterns highlights partial conversion of the WS_2 elements to $WO_3{\cdot}H_2O$. However, in this sample, only two out of fours peaks identified in the GO/WS_2 mixture are picked up during the analyses. The result suggests that relative to the GO/WS_2 mixture, by increasing the temperature of the GO and WS_2 mixture to 85 °C (in ambient), the process encourages W to be readily oxidized into WO_3 and form bonds with water molecules. These water molecules are present on the surface and trapped between the GO flakes. As a result, S atoms will likely remain within and on the surface of the GO-H_2O film mixture. From the above analyses, these nanocubes will now be termed WO_3 nanocubes.

WO_3 Nanocubes as Beacons for Enhancement of Silver Dendrites' Formation. In a bid to determine the potential use of the WO_3 nanocubes as beacons to facilitate the formation of silver dendrites in the presence of an applied potential, 8 μL of $AgNO_3$ solution is deposited across the hybrid film for 20s in a dark environment, with minimum light being introduced onto the sample. The choice of a dark environment minimizes any chances of photoreduction of $AgNO_3$, thus allowing results from subsequent electrochemical processes to be more accurately presented.

https://doi.org/10.1021/acsomega.1c06963
ACS Omega 2022, 7, 10330–10339

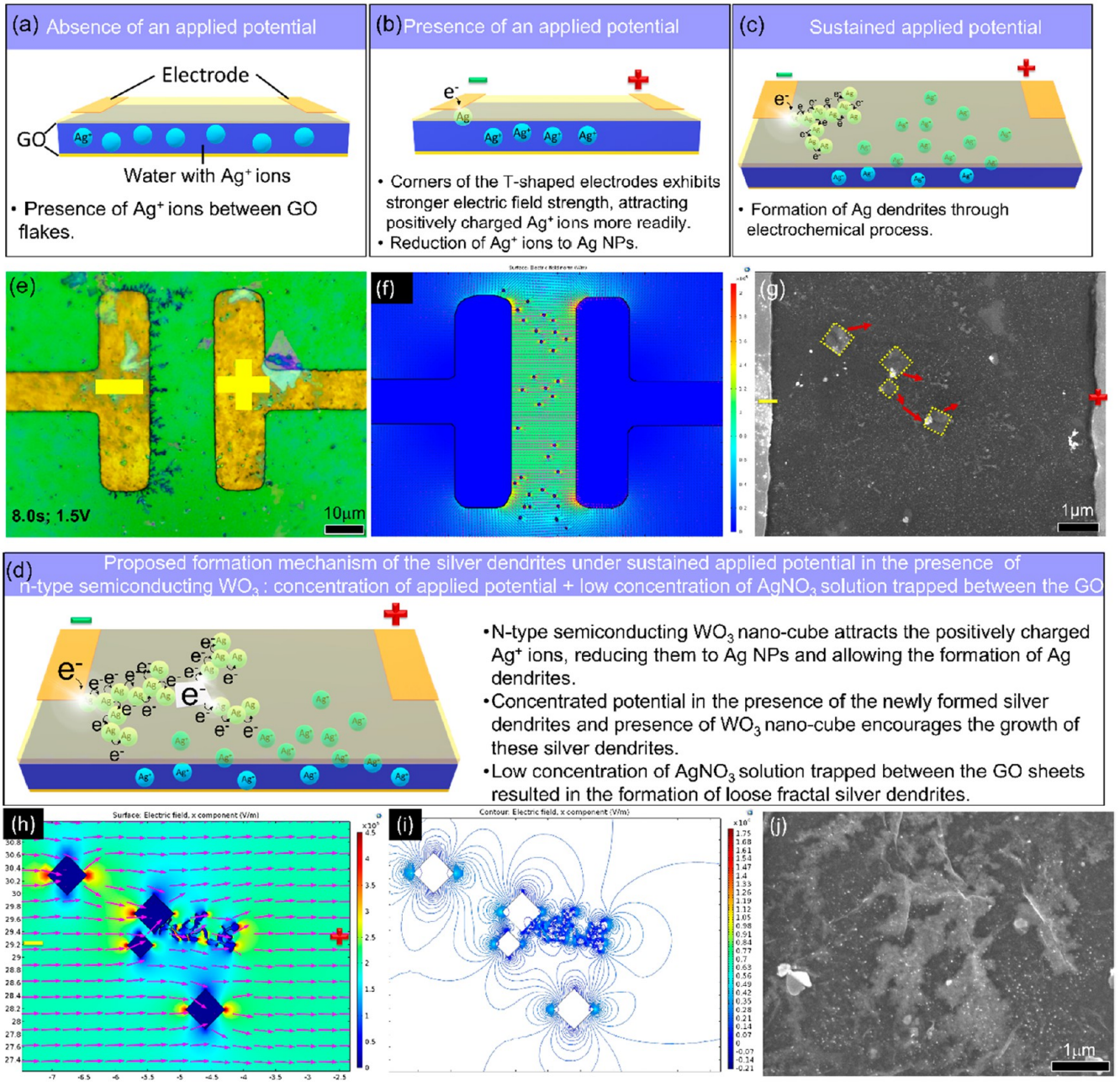

Figure 5. (a–d) Illustrates the formation process of Ag dendrites through the electrochemical method, and how the presence of WO_3 nanocubes can further encourage while influencing the formation and paths of these Ag dendrites. (e) Time-lapsed optical image of Ag dendrites formation across T-shaped electrodes after applying 1.5 V for 8 s. (g) SEM image of four WO_3 nanocubes highlighted by yellow dotted lines and the red arrows indicates the growth direction of Ag dendrites from the WO_3 nanocubes. (f, h, i) COMSOL simulation of how the electric field distribution across the electrodes is affected by the WO_3 nanocubes and the growth of Ag dendrites. The location of the nanocubes and Ag dendrites in the simulation matches those in (e) and (g), respectively. (j) A higher-magnification SEM view of the loose fractal formation of Ag dendrites obtained through our process.

Subsequently, the sample is rinsed with deionized water and blown dry with nitrogen gas. The seemingly dried sample is then connected to a source meter to study Ag dendrites formation via electrochemical migration process across the composite film. The fabrication process, as mentioned above, is depicted in Figure 3a.

When a constant potential is applied between the electrodes, the growth of Ag dendrites takes place from both corners of the T-shape negative electrode Figure 3c through an electrochemical deposition process. In general, Ag^+ ions electrolytes provided by $AgNO_3$ solutions are trapped between the GO flakes. These Ag^+ ions then take in electrons from the cathode in the presence of an applied potential. The process results in the formation of Ag nanoparticles at the interface between water and the cathode. Ag^+ ions are continuously being reduced, and the Ag dendrites are formed by maintaining a constant potential, hence a constant supply of electrons. A detailed study of Ag dendrites' formation on pristine GO flakes has been reported by Leow et al.[21] The growth of Ag dendrites begins from the corner of the T-shaped electrodes due to the

https://doi.org/10.1021/acsomega.1c06963
ACS Omega 2022, 7, 10330–10339

presence of a stronger electric field present at these locations. The above statement is justified by the COMSOL simulation of electric field (indicated by the white cones) across parallel electrodes under an applied potential of 1.5 V, as presented in Figure 3b.

Pristine GO flakes are replaced with the GO/WO_3 film while maintaining a similar electrode design and applied potential. Because of the replacement, a unique growth path for the Ag dendrite is observed over such film (Figure 3g). The first instant potential is applied across the electrodes; no dendrite growth is observed to form between the parallel portion of the electrodes on the GO film (Figure 3c). However, in the case where WO_3 nanocubes are present on the GO film, short dendrites have already started to form under the same circumstances. As Ag dendrites migrate across the composite film, they travel along a preferential path toward the WO_3 nanocubes, which likely serve as beacons (Figure 3h) to guide the formation of Ag dendrites. Upon coming into contact, these nanocube beacons triggered the formation of more Ag dendrites. By maintaining a constant applied potential of 1.5 V, more bunching of Ag dendrites from the WO_3 nanocube beacons is observed Figure 3i,j. In the absence of the WO_3 nanocubes (Figure 3c–f), the duration of the applied field required to achieve the same distance of the migration process is much longer. The observation further highlights the directive role of the WO_3 nanocubes.

The role of WO_3 nanocubes in enhancing Ag dendrites formation is verified by covering the bottom half of the electrodes with a PDMS polymer layer (region highlighted by the black dotted line in Figure 4a) before allowing the top half to be decorated with WO_3 nanocubes. The nanocubes are enclosed by the white circles in Figure 4a. For the same amount and duration of applied potential, it is noticeable that the growth of these Ag dendrites (highlighted by the red arrows in Figure 4a–f) takes place primarily within the region where WO_3 nanocubes are present, and these dendrites are "attracted" toward these WO_3 nanocubes. The observation thus affirms the above-proposed role played by these WO_3 nanocubes. By changing the design of the electrode, replacing one of the T-shaped electrodes with a pointed edge, the distributions of the electric field are changed. As a result, the effect of WO_3 on the growth of the Ag dendrites becomes more substantial. Figure 4g–h shows the growth of Ag dendrites from the pointed electrode across pristine GO film. These dendrites branch out from the pointed tip, as well as the edges of the pointed electrode. In the presence of WO_3 nanocubes, it is evident that the Ag dendrites grow from the pointed growth of Ag dendrites along the edges of the sharp electrode. In the presence of WO_3 nanocubes, it is evident that the Ag dendrites grow from the pointed growth of Ag dendrites along the edges of the sharp electrode.

Proposed Mechanism of WO_3 Nanocubes's Role in Directing Ag Dendrites' Formation. The electrochemical method for controlled synthesis of silver dendrites is a well-established process.[17,21,29] It involves tuning the applied electric potential to create an inequilibrium thermodynamic environment that favors the reduction of Ag^+ ions, resulting in the formation of Ag dendrites. In a similar context, Figure 5a–d illustrates how Ag dendrites are readily formed in this work. In the absence of an applied electric potential, low concentrations of Ag^+ ions in water are trapped between the GO flakes.[21] Applying an electric potential across the T-shaped electrodes generates a stronger electric field around the corners (a claim supported by COMSOL simulation of electric field lines between two T-shaped electrodes (Figure 3b and Figure 5f). Consequently, a combinatory effect of strong electric field coupled with low concentrations of Ag^+ ions, resulted in the free-roaming positively charged Ag^+ ions to become more strongly attracted to the corners of the negative electrodes and become reduced.[30] The process then results in the formation of Ag dendrites, branching out from the electrode corners more readily than other parts of the electrodes (Figure 5b,e) through an ion diffusion limited growth process.[30,31] With sustained applied electric potential, a continuous reduction of Ag^+ ions to Ag NPs takes place, extending these Ag dendrites toward the positive electrode (Figure 5c).

Previous work by Leow et al.[21] underscored the ability to direct and control the migrating path of Ag nanoparticles across GO by using a focused laser beam to tune the electron affinity of the GO film and directing the electric field across the GO film, while You et al.[30] showcased how *in situ* studies of growth modes of silver crystals are induced by the presence of a concentrated field in an aqueous solution. Both works highlight the critical role electric field distribution has in shaping the direction in which Ag nanoparticles migration can occur.

Single-crystal WO_3 is an n-type semiconductor,[32] which means that the positively charged Ag^+ ions will naturally be attracted to these negatively charged beacons. Under the influence of a constant applied electric potential, these WO_3 nanocubes then readily reduced the Ag^+ ions, allowing Ag dendrites to start branching out from these WO_3 nanocubes.

Not only so, in the presence of an applied potential, electric field distribution will also be affected by both the orientations and locations of these nanocubes (Figure 5h). The above statement is justified through COMSOL simulation. A time-lapse optical image of Ag dendrites growth across T-shaped electrodes under an applied potential of 1.5 V for 8 s was captured, and the positions of the nanocubes, appearing as white specks, are recorded in Figure 5e. The geometry is then duplicated in COMSOL simulation, and an electric field distribution under similar applied potential is presented in Figure 5f. In Figure 5f, magenta arrows indicate how localized electric field lines are redistributed around the WO_3 nanocubes. A close-up SEM image of typical Ag dendrites growth (red arrow) around the WO_3 nanocubes (yellow dotted box) is depicted in Figure 5g. Running similar COMSOL simulation reveals how the Ag dendrites' growth direction from the WO_3 nanocubes accords with the alterations to the electric field distributions (Figure 5h). As the Ag dendrites extend from the WO_3 nanocube, the surface and contour plot of the potential from the simulation emphasized how the concentrated potential field around the Ag dendrites can further encourage the formation of more bunches (Figure 5h,i). A higher magnification SEM view of the Ag dendrites formed through this process shows loose fractal formation. The observation is in good agreement with the proposal by You et al.,[30] given our work also utilizes low concentrations of Ag^+ ions and a concentrated field by both the WO_3 nanocubes and newly formed Ag dendrites.

Unique Function of S Atoms. Previously, Raman analysis suggested the formation of $WO_3{\cdot}H_2O$ elements upon thermal annealing of GO and WS_2 mixture to 85 °C (in ambient). Coupled with electrical measurements and COMSOL simulation, the role of the WO_3 nanocube as a guiding beacon is now better understood. However, that leaves an unsolved

https://doi.org/10.1021/acsomega.1c06963
ACS Omega 2022, 7, 10330−10339

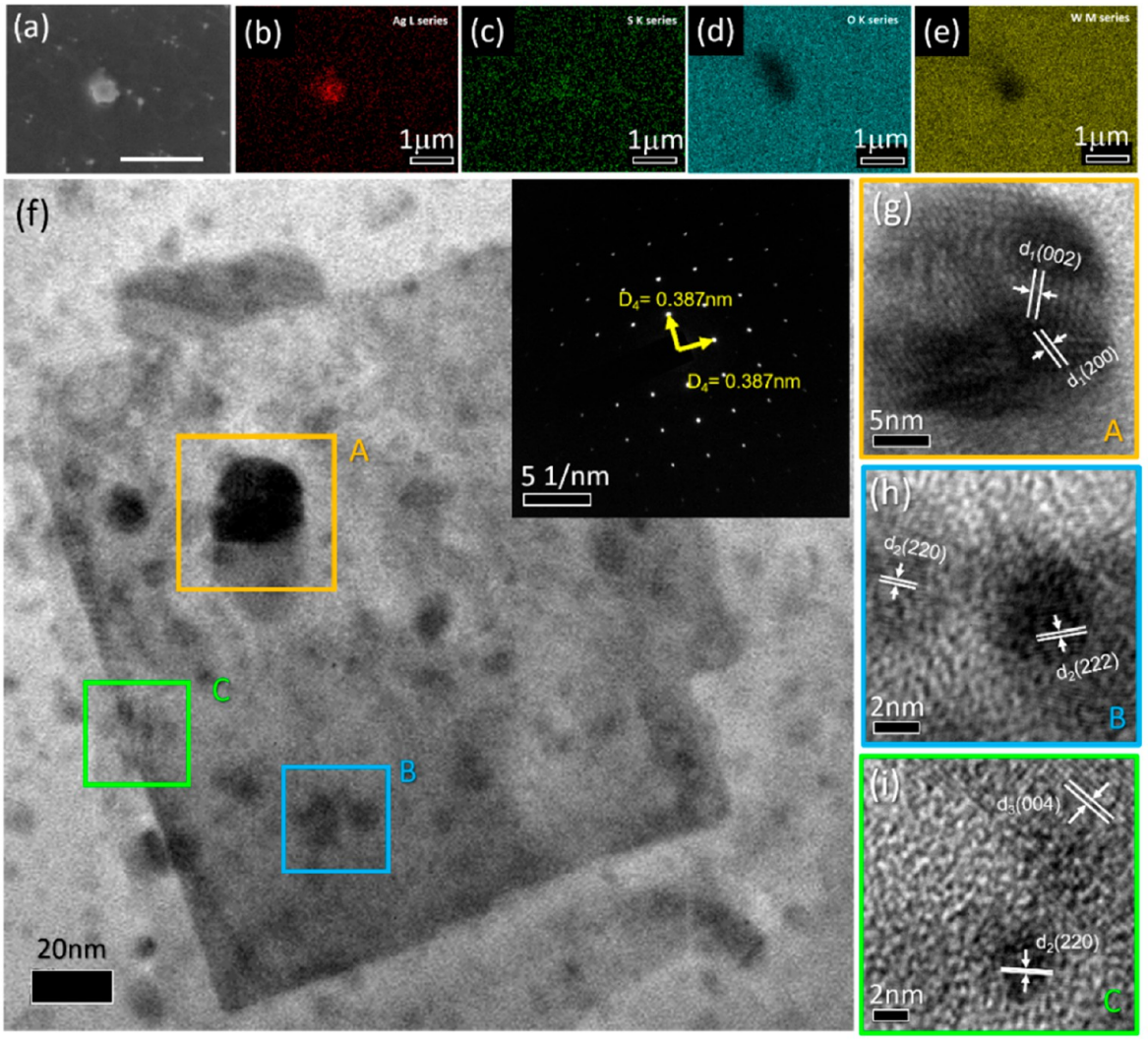

Figure 6. (a–e) EDX elemental maps of one WO_3 nanocube after applying an electric field. (f) TEM image of a WO_3 nanocube decorated with AgS NPs. Inset is a SAED of the WO_3 nanocube. (g–i) HRTEM of (g) orange, (h) blue, and (i) green regions highlighted in (f). d_1, d_2, and d_3 represent the interplanar distance of $Ag_2(HSO_4)_2(H_2SO_4)$, AgS, and WO_3.

puzzle about the role played by S atoms. With the oxidation of W to form WO_3, S atoms from WS_2 precursors are believed to have likely remained within and on the surface of the composite film.

Thorough SEM and EDX elemental maps of these nanocubes insinuate the possible formation of AgS on the surface of the nanocubes (Figure 6a–e). A more comprehensive analysis of these nanocubes after the migration process is conducted using HRTEM (Figure 6f–i). The TEM image presented in Figure 6f shows the formation of small NPs on a single nanocube. SAED characterization of the cube produces a cubic atomic structure with an interplanar distance of 0.387 nm (inset of Figure 6f). The result corresponds to that of WO_3,[33] which is in good agreement with the Raman results.

To determine the nature of these NPs atop the nanocube, HRTEM reveals lattice structures corresponding to two different compositions. From the region enclosed by the orange square in Figure 6f, the lattice spacing (Figure 6g) of 0.712 and 0.498 nm matches the (002) and (200) plane of silver hydrogen sulfate, $Ag_2(HSO_4)_2(H_2SO_4)$.[34] From the smaller region in the blue square (Figure 6f), these nanoparticles are identified as silver sulfide, AgS composites with the lattice spacing of 0.207 and 0.188 nm (Figure 6h). These spacings correspond to the lattice planes (220) and (222). From the third region enclosed in the green square (Figure 6f), the nanoparticle is identified to be AgS with the lattice plane (220), while the surface on which the nanoparticle formed is WO_3 with lattice plane (004) (Figure 6i).

Results from the HRTEM analysis suggest that under an applied electric potential, Ag ions react with S ions on the WO_3 nanocubes to form AgS NPs. At the same time, these Ag ions could also be intercalated within the WO_3 nanostructure. The intercalation process is highly dependent on the crystal structure of the WO_3 nanocubes. In general, the higher symmetry of the crystalline will bring about a greater possibility for ion intercalation.[35] Since the WO_3 nanocubes are identified to have a cubic phase crystal structure (inset Figure 6f), it provides a favorable condition for this process.

Despite the formation of AgS NPs atop these WO_3 nanocubes, SEM and EDX analysis suggest that the dendrites branching out from these WO_3 nanocubes beacons comprise mainly Ag NPs. Figure 7a shows an SEM image of the dendrites formed between the electrodes after applying an electric potential. EDX spectra (Figure 7b–d) obtained from

https://doi.org/10.1021/acsomega.1c06963
ACS Omega 2022, 7, 10330–10339

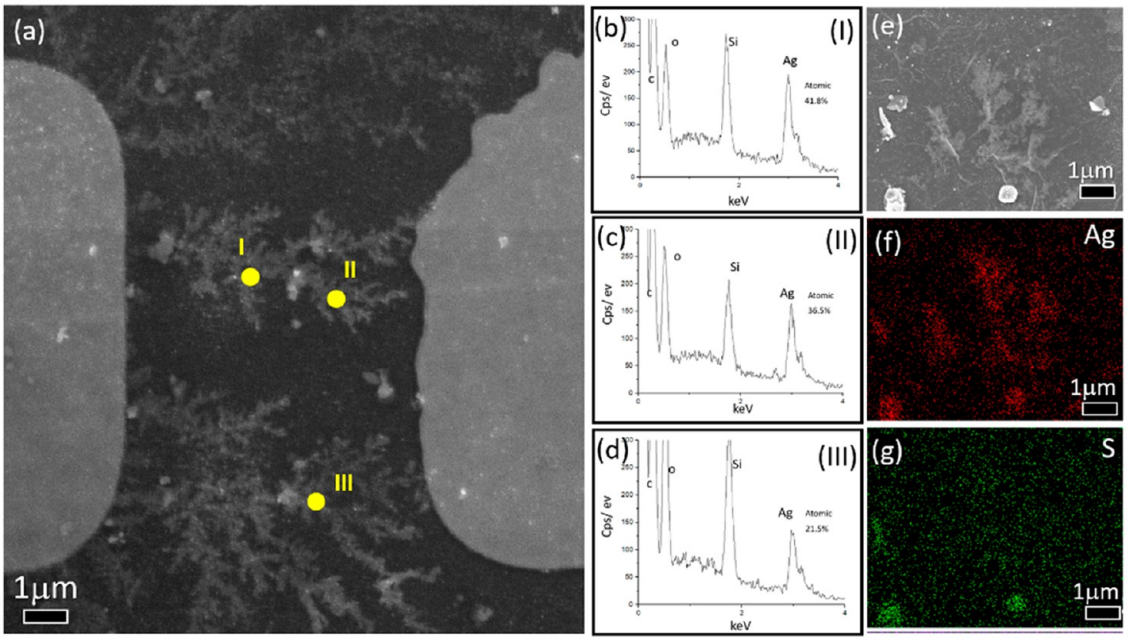

Figure 7. (a) SEM image of silver dendrites formed across electrodes. (b–d) EDX spectra of regions I, II, and III indicated in (a). (e–g) EDX elemental map of the dendrites showing that the dendrites comprise Ag atoms.

the dendrites, indicated as I, II, and III in (Figure 7a), suggest that these dendrites mainly comprise Ag NPs. This result is further verified by the elemental map of silver and sulfur (Figure 7e–g).

CONCLUSIONS

Herein, we report success in utilizing WO_3 nanocubes as guiding beacons to encourage the synthesis and direct the growth of Ag dendrites. Using a simple mixing and low-temperature heating process, WS_2, in the presence of GO suspension, formed W–O–W and W–OH_2 bonds. These bonds are representative of $WO_3 \cdot H_2O$ elements. When dispersed together with GO microflakes to form a thin composite film, these WO_3 nanocubes readily alter electric field distribution under an applied potential. Depending on their location and orientation, the site-specific concentration of the electric field initiates Ag dendrites' growth from these sites. This claim is justified through Multiphysics COMSOL simulation. At the same time, the WO_3 nanocubes also serve as path-guiding beacons, encouraging more growth of Ag dendrites within a shorter time. Simultaneously, sulfur from the dissociation of WS_2, when left to interact with the Ag ions, resulted in the formation of AgS and $Ag_2(HSO_4)_2(H_2SO_4)$ nanoparticles atop the WO_3 nanocubes. Because of the cubic phase of WO_3, there is also a likelihood of intercalating these nanoparticles within the nanocubes. Thus, our work presented a new and straightforward approach to encourage and direct the growth of Ag dendrites through an electrochemical migration process.

EXPERIMENTAL METHODS

Sample Preparation. *Graphene Oxide and Tungsten Disulfide Mixture.* Highly concentrated graphene oxide (GO) microflakes (6 M L^{-1}, Graphene Supermarket) are diluted to 2 M L^{-1}. The diluted solution is mixed with tungsten disulfide microflakes solution (WS_2, Graphene supermarket) to a 1:5 volume ratio.

Oxygen Etching of SiO_2/Si Substrate and Preparation of Silver Nitrate Solution. Patterned SiO_2/Si substrates undergo reactive ion etching at 200W for 1 min with 50 ccm of oxygen to enhance the substrate's hydrophilicity for better GO deposition. A silver nitrate solution is obtained by dissolving silver nitrate crystals (Sigma-Aldrich) in deionized water to a concentration of 0.1 M L^{-1}.

Fabrication of Gold Electrodes on SiO_2/Si. The electrodes' fabrication was achieved using UV lithography and sputtering metal deposition. Soda-lime blank (Nanofilm, Wetlake Village, California) with 100 nm thick chromium and 530 nm thick layer of AZ1518 photoresist is patterned by a direct-write laser system (Heidelberg Instruments uPG 101) to fabricate the initial UV photomask with electrode patterns. Next, a 1 μm thick AZ1512 resist is deposited by spin coating and being exposed to UV light in a Mask & Bond Aligner (Karl Suss, MA8/BA6). After resist development, two layers of Cr/Au (10 nm/50 nm) are sputtered on the SiO_2/Si substrates as an adhesion and electrode base, respectively. Finally, lift-off is carried out using acetone, leaving the electrodes on the SiO_2/Si wafer (Nanyang Equipment Pte Ltd.).

Further Characterizations. Further characterizations are carried out using an optical microscope (OM) (model: Olympus BX51) under bright field illumination. Surface morphology, crystallinity, and chemical composition are characterized using SEM-EDX (JEOL JSM6700-F with Oxford Instruments X-Max^N 150 EDX detector) and TEM (JEOL JEM-2010F). Raman measurement is carried out using a Renishaw System coupled with a 532 nm laser. Electrical measurements are conducted using the Keithley 4200-SCS Source-meter unit attached to the OM.

https://doi.org/10.1021/acsomega.1c06963
ACS Omega 2022, 7, 10330–10339

AUTHOR INFORMATION

Corresponding Authors

Chorng-Haur Sow − *Department of Physics, National University of Singapore, Singapore 117542, Singapore; Center For Advanced 2D Materials and Graphene Research Center, National University of Singapore, Singapore 117546, Singapore;* orcid.org/0000-0001-6385-3017; Phone: (+65) 65162957; Email: physowch@nus.edu.sg; Fax: (+65) 67776126

Sharon Xiaodai Lim − *Department of Physics, National University of Singapore, Singapore 117542, Singapore;* orcid.org/0000-0001-9198-8998; Phone: (+65) 65161161; Email: phylimx@nus.edu.sg

Author

Lu Gan − *Department of Physics, National University of Singapore, Singapore 117542, Singapore; Jianqing Experiment School, Shanghai 10312, China*

Complete contact information is available at: https://pubs.acs.org/10.1021/acsomega.1c06963

Author Contributions

The manuscript was written through the contributions of all authors. All authors have approved the final version of the manuscript.

Notes

The authors declare no competing financial interest.

ACKNOWLEDGMENTS

The authors acknowledge the generous support of Singapore MOE-ARC grant (R-144-000-393-114). The authors would like to thank Dr. Wu Jian Feng for his kind assistance in electrode fabrication.

REFERENCES

(1) Lim, S. X.; Lee, Y. Z.; Gao, N.; Lu, J.; Xu, Q.; Tok, E. S.; Sow, C. H. Templating nanotraffic light - dynamic tricoloured blinking silver nanoclusters on a graphene oxide film. *Journal of Materials Chemistry C* **2018**, *6*, 4641.

(2) Lim, S. X.; Zhang, Z.; Koon, G. K. W.; Sow, C. H. Unlocking the potential of carbon incorporated silver-silver molybdate nanowire with light. *Applied Materials Today* **2020**, *20*, 100670.

(3) Fan, J. G.; Zhao, Y. P. Freezing a water droplet on an aligned Si nanorod array substrate. *Nanotechnology* **2008**, *19*, 155707.

(4) Qian, L.; Yang, X. R. Dendrimers as "controllers" for modulation of electrodeposited silver nanostructures. *Colloids and Surfaces a-Physicochemical and Engineering Aspects* **2008**, *317*, 528.

(5) Fu, L.; Zhu, D. M.; Yu, A. M. Galvanic replacement synthesis of silver dendrites-reduced graphene oxide composites and their surface-enhanced Raman scattering characteristics. *Spectrochimica Acta Part a-Molecular and Biomolecular Spectroscopy* **2015**, *149*, 396.

(6) Zhou, Q.; Wang, S.; Jia, N. Q.; Liu, L.; Yang, J. J.; Jiang, Z. Y. Synthesis of highly crystalline silver dendrites microscale nanostractures by electrodeposition. *Mater. Lett.* **2006**, *60*, 3789.

(7) Rafatmah, E.; Hemmateenejad, B. Dendrite gold nanostructures electrodeposited on paper fibers: Application to electrochemical non-enzymatic determination of glucose. *Sensors and Actuators B-Chemical* **2020**, *304*, 127335.

(8) Zhang, X. J.; Wang, G. F.; Liu, X. W.; Wu, H. Q.; Fang, B. Copper dendrites: Synthesis, mechanism discussion, and application in determination of L-tyrosine. *Cryst. Growth Des.* **2008**, *8*, 1430.

(9) Qin, Y.; Song, Y.; Sun, N. J.; Zhao, N.; Li, M. X.; Qi, L. M. Ionic liquid-assisted growth of single-crystalline dendritic gold nanostructures with a three-fold symmetry. *Chem. Mater.* **2008**, *20*, 3965.

(10) Zhou, P.; Dai, Z. H.; Fang, M.; Huang, X. H.; Bao, J. C.; Gong, J. F. Novel dendritic palladium nanostructure and its application in biosensing. *J. Phys. Chem. C* **2007**, *111*, 12609.

(11) Gu, C. D.; Zhang, T. Y. Electrochemical Synthesis of Silver Polyhedrons and Dendritic Films with Superhydrophobic Surfaces. *Langmuir* **2008**, *24*, 12010.

(12) Xie, S. P.; Zhang, X. C.; Xiao, D.; Paau, M. C.; Huang, J.; Choi, M. M. F. Fast Growth Synthesis of Silver Dendrite Crystals Assisted by Sulfate Ion and Its Application for Surface-Enhanced Raman Scattering. *J. Phys. Chem. C* **2011**, *115*, 9943.

(13) GunaVathana, S. D.; Thivya, P.; Wilson, J.; Peter, A. C. Sensitive voltammetric sensor based on silver dendrites decorated polythiophene nanocomposite: Selective determination of L-Tryptophan. *J. Mol. Struct.* **2020**, *1205*, 127649.

(14) Sharma, D. K.; Ott, A.; O'Mullane, A. P.; Bhargava, S. K. The facile formation of silver dendritic structures in the absence of surfactants and their electrochemical and SERS properties. *Colloids and Surfaces a-Physicochemical and Engineering Aspects* **2011**, *386*, 98.

(15) Gladitz, M.; Reinemann, S.; Radusch, H. J. Preparation of Silver Nanoparticle Dispersions via a Dendritic-Polymer Template Approach and their Use for Antibacterial Surface Treatment. *Macromol. Mater. Eng.* **2009**, *294*, 178.

(16) Jeon, H.; Joo, J.; Kwon, Y.; Uhm, S.; Lee, J. Morphological features of electrodeposited Pt nanoparticles and its application as anode catalysts in polymer electrolyte formic acid fuel cells. *J. Power Sources* **2010**, *195*, 5929.

(17) Fu, L.; Tamanna, T.; Hu, W. J.; Yu, A. M. Chemical preparation and applications of silver dendrites. *Chemical Papers* **2014**, *68*, 1283.

(18) Bahadori, S. R.; Mei, L. Y.; Athavale, A.; Chiu, Y. J.; Pickering, C. S.; Hao, Y. W. New Insight into Single-Crystal Silver Dendrite Formation and Growth Mechanisms. *Cryst. Growth Des.* **2020**, *20*, 7291.

(19) Osminkina, L. A.; Zukovskaja, O.; Agafilushkina, S. N.; Kaniukov, E.; Stranik, O.; Gonchar, K. A.; Yakimchuk, D.; Bundyukova, V.; Chermoshentsev, D. A.; Dyakov, S. A.; et al. Gold nanoflowers grown in a porous Si/SiO2 matrix: The fabrication process and plasmonic properties. *Appl. Surf. Sci.* **2020**, *507*, 144989.

(20) Yakimchuk, D. V.; Kaniukov, E. Y.; Lepeshov, S.; Bundyukova, V. D.; Demyanov, S. E.; Arzumanyanm, G. M.; Doroshkevich, N. V.; Mamatkulov, K. Z.; Bochmann, A.; Presselt, M.; et al. Self-organized spatially separated silver 3D dendrites as efficient plasmonic nanostructures for surface-enhanced Raman spectroscopy applications. *J. Appl. Phys.* **2019**, *126*, 233105.

(21) Leow, Y. H. J.; Lim, P. Y. X.; Lim, S. X. D.; Wu, J. F.; Sow, C. H. Nanosurfer flash-mobs: electric-field-choreographed silver migration on graphene oxide. *Nanoscale Advances* **2019**, *1*, 2180.

(22) Sun, P. X.; Cao, Z.; Zeng, Y. X.; Xie, W. W.; Li, N. W.; Luan, D.; Yang, S.; Yu, L.; Lou, X. W. D. Formation of Super-Assembled TiOx/Zn/N-Doped Carbon Inverse Opal Towards Dendrite-Free Zn Anodes. *Angew. Chem., Int. Ed.* **2022**, *61*, e202115649.

(23) Dhanush, S.; Sreejesh, M.; Bindu, K.; Chowdhury, P.; Nagaraja, H. S. Synthesis and electrochemical properties of silver dendrites and silver dendrites/rGO composite for applications in paracetamol sensing. *Mater. Res. Bull.* **2018**, *100*, 295.

(24) Xiu, L. Y.; Wang, Z. Y.; Qiu, J. S. General synthesis of MXene by green etching chemistry of fluoride-free Lewis acidic melts. *Rare Metals* **2020**, *39*, 1237.

(25) Yan, X. H.; Dai, Y.; Chen, M.; Wang, J. J.; Ren, J.; Wang, Q.; Wu, Y. Z.; Ye, N. F.; Wang, Y. P.; Cheng, X. N. WS2 nanosheets decorated by Ag nanoparticles with different content and uniform distribution for enhanced electrochemical properties. *J. Nanopart. Res.* **2017**, *19*, 165.

(26) Lim, S. X.; Koon, G. K. W.; Zhan, D.; Shen, Z. X.; Ozyilmaz, B.; Sow, C. Assembly of suspended graphene on carbon nanotube scaffolds with improved functionalities. *Nano Research* **2012**, *5*, 783.

(27) Peimyoo, N.; Shang, J. Z.; Yang, W. H.; Wang, Y. L.; Cong, C. X.; Yu, T. Thermal conductivity determination of suspended mono- and bilayer WS2 by Raman spectroscopy. *Nano Research* **2015**, *8*, 1210.

(28) Daniel, M. F.; Desbat, B.; Lassegues, J. C.; Gerand, B.; Figlarz, M. Infrared and Raman-Study of WO_3 Tungsten Trioxides and WO_3, xH_2O Tungsten Trioxide dehydrates. *J. Solid State Chem.* **1987**, *67*, 235.
(29) Fu, L.; Lai, G. S.; Mahon, P. J.; Wang, J.; Zhu, D. M.; Jia, B. H.; Malherbe, F.; Yu, A. M. Carbon nanotube and graphene oxide directed electrochemical synthesis of silver dendrites. *Rsc Advances* **2014**, *4*, 39645.
(30) You, H. J.; Ding, C. H.; Song, X. P.; Ding, B. J.; Fang, J. X. In situ studies of different growth modes of silver crystals induced by the concentration field in an aqueous solution. *CrystEngComm* **2011**, *13*, 4491.
(31) You, H. J.; Fang, J. X.; Chen, F.; Shi, M.; Song, X. P.; Ding, B. J. Morphological Evolution of Fractal Dendritic Silver Induced by Ions Walking within the Diffusion Layer. *J. Phys. Chem. C* **2008**, *112*, 16301.
(32) Hirose, T.; Kawano, I.; Niino, M. Electrical conductivity of Tungsten Trioxide (WO_3). *J. Phys. Soc. Jpn.* **1972**, *33*, 272.
(33) Tokunaga, T.; Kawamoto, T.; Tanaka, K.; Nakamura, N.; Hayashi, Y.; Sasaki, K.; Kuroda, K.; Yamamoto, T. Growth and structure analysis of tungsten oxide nanorods using nvironmental TEM. *Nanoscale Res. Lett.* **2012**, *7*, 3921.
(34) Stiewe, A.; Kemnitz, E.; Troyanov, S. Synthese und Kristallstruktur von Hydrogensulfaten einwertiger Metalle−$Ag(H_3O)$-$(HSO_4)_2$, $Ag_2(HSO_4)_2(H_2SO_4)$, $AgHSO_4$ und $Hg_2(HSO_4)_2$. *Zeitschrift für anorganische und allgemeine Chemie* **1999**, *625*, 329.
(35) Mandal, D.; Routh, P.; Nandi, A. K. A New Facile Synthesis of Tungsten Oxide from Tungsten Disulfide: Structure Dependent Supercapacitor and Negative Differential Resistance Properties. *Small* **2018**, *14*, 1702881.

https://doi.org/10.1021/acsomega.1c06963
ACS Omega 2022, 7, 10330−10339